University of South Carolina College of Engineering and Computing Mechanical Engineering Department

Flow boiling phenomena in a single annular flow regime in microchannels (II): Reduced pressure drop and enhanced critical heat flux

Fanghao Yang, Xianming Dai, Yoav Peles, Ping Cheng, Jamil Khan, Chen Li

International Journal of Heat and Mass Transfer 68 (2014) 716–724

Contents lists available at ScienceDirect

International Journal of Heat and Mass Transfer

journal homepage: www.elsevier.com/locate/ijhmt

Flow boiling phenomena in a single annular flow regime in microchannels (II): Reduced pressure drop and enhanced critical heat flux

Fanghao Yang [a], Xianming Dai [a], Yoav Peles [b], Ping Cheng [c], Jamil Khan [a], Chen Li [a,*]

[a] Department of Mechanical Engineering, University of South Carolina, 300 Main St, Columbia, SC 29208, USA
[b] Department of Mechanical, Aerospace & Nuclear Engineering, Rensselaer Polytechnic Institute, 110 8th St, Troy, NY 12180, USA
[c] School of Mechanical and Power Engineering, Shanghai Jiaotong University, 800 Dong Chuan Rd, Shanghai 200240, China

ARTICLE INFO

Article history:
Available online 17 October 2013

Keywords:
Single annular flow
Microchannel
Superhydrophilic silicon nanowire
Pressure drop
Critical heat flux

ABSTRACT

In Part II of this study, we report that pressure drop was reduced by approximately 48% and critical heat flux (*CHF*) was increased by approximately 300% in *SiNW* microchannels compared to these in smooth wall microchannels. The hydraulic characteristics of the single annular flow were systematically investigated to reveal the mechanisms responsible for the reduced pressure drop and enhanced *CHF*. In the single annular regime, the liquid and vapor flows were nearly fully separated during the entire flow boiling process (i.e., from the onset of nucleate boiling to the *CHF* conditions). Moreover, the entrainment droplets were reduced by flattening the profile of the liquid–vapor interfaces using the high capillary pressure generated by *SiNWs*. These two factors, i.e., flow separation and reduced entrainment droplets, lead to a dramatic reduction of frictional pressure drop. The separation of liquid and vapor flows as well as the improved global and local liquid supply result in a significant *CHF* enhancement without using inlet restrictors (*IR*). Reynolds number based the vapor flow at the exit ranged from 0.1 to 2100.

1. Introduction

Technically, flow boiling in microchannels has several key advantages over single-phase liquid heat transfer including higher heat transfer coefficient, a more uniform surface temperature, lower mass flux, and potentially lower pressure drop/pumping power (because of the low mass flux). However, for a given mass flux, the pressure drop of two-phase flow is significantly higher than single phase flow primarily because of the reduced fluid density and increased kinematic viscosity [1,2]. Moreover, flow boiling instabilities often cause premature critical heat flux (*CHF*) conditions [3]. Several techniques such as inlet restrictors (*IRs*) [4–6], seed bubbles [7–9], self-sustained high frequency two-phase oscillations [10,11], and diverging cross-section channels [12–15] were developed to suppress flow boiling instabilities and hence to enhance *CHF*. *IRs* are one of the most effective methods to mitigate these instabilities [4,16,17], however, they lead to a significant increase in pressure drop [4,16,18] (as shown in Fig. 1). Existing studies indicate that roughness [19–21] and wettability [22–24] of the channel surfaces play important roles in determining the thermal-hydraulic characteristics of two-phase flows. It was shown that capillary forces can affect pressure drop in microchannels, which can be reduced by increasing surface wettability [22,23]. However, this can be only achieved at low vapor qualities, i.e., $\chi < 0.08$, and low flow rates. Additionally, *CHF* was observed to be enhanced using high-roughness microscale wicking structures in microchannel [20,21,24]. The capillarity resulting from superhydrophilic wicking structures was believed to be the primary reason. However, higher wall roughness can also induce higher pressure drop [19]. It is still necessary to improve and develop new methods to enhance *CHF* and effectively manage pressure drops in microchannels by directly manipulating two-phase flow regimes or flow structures [21,25,26].

Compared to microchannels with smooth walls, the pressure drop was substantially reduced and the *CHF* conditions were greatly enhanced without using *IRs*. Compared to microchannels with *IRs*, *CHF* was slightly reduced at high mass fluxes. The improved liquid supply to the boiling surfaces, which was enabled by local liquid spreading via capillarity in superhydrophilic silicon nanowires (*SiNWs*), primarily results in a significant enhancement of *CHF*. Visualization and theoretical analysis reveal that a new flow structure in the form of nearly ideal separation of vapor and

* Corresponding author.
E-mail address: li01@mailbox.sc.edu (C. Li).

0017-9310/$ - see front matter © 2013 Elsevier Ltd. All rights reserved.
http://dx.doi.org/10.1016/j.ijheatmasstransfer.2013.09.060

Nomenclature

A	area, m^2
C_c	parameter for exit effect
C_f	frictional coefficient
D	diameter, m
H	height, m
h_{fg}	latent heat of vaporization, kJ/kg
f	fanning friction factor
G	mass flux, kg/m^2 s
K_d	momentum correction factor
L	length, m
$\dot{m}$	mass flow rate, kg/s
N	number of pin fins
Δp	pressure drop, N/m^2
P	power, W
S	slip coefficient
S_T	transverse pitch, m
u	velocity, m/s
$\bar{u}$	average velocity, m/s
W	microchannel width, m
z	coordinate, m
Greek symbols	
α	void fraction
γ	surface tension, N/m
θ	contact angle
μ	viscosity, kg/(s m)
ρ	density, kg/m^3
χ	vapor quality
σ_i	interfacial stress, N/m^2
τ	flow area contraction ratio
Subscripts	
2ϕ	two-phase
acc	accelerational
c	cross-sectional
CHF	critical heat flux
e	exit
eff	effective
exp	experimental
f	frictional
h	hydraulic
i	inlet
l	liquid
m	mixture
o	outlet
sat	saturated
v	vapor

liquid flows as well as flattened profiles of liquid–vapor interfaces determine the significant reduction of pressure drop.

2. Data reduction

Experimental frictional pressure drop, $\Delta p_{f,\exp}$, was reduced from the following equation:

$$\Delta p_{f,\exp} = \Delta p_{total} - \Delta p_{acc} - \Delta p_i - \Delta p_o - \Delta p_{plenum} - \Delta p_{distributor} \quad (1)$$

where accelerational pressure drop, Δp_{acc}, is given by:

$$\Delta p_{acc} = G^2\left(\frac{1}{\rho_i} - \frac{1}{\rho_{2\phi,o}}\right) \quad (2)$$

where $\Delta p_{distributor}$, Δp_{plenum}, Δp_i, and Δp_o are the pressure drop of the flow distributor, pressure drop of the plenum chambers, inlet minor losses, and exit minor losses; the total pressure drop, Δp_{total}, was measured by two pressure transducers at pressure-drop measuring ports; the mass flux was estimated from $G = \dot{m}/A_c$. ρ_l and ρ_v denote the densities of liquid and vapor, respectively; and the density of the inlet flow, ρ_i, is assumed to be the density of liquid flow, ρ_l.

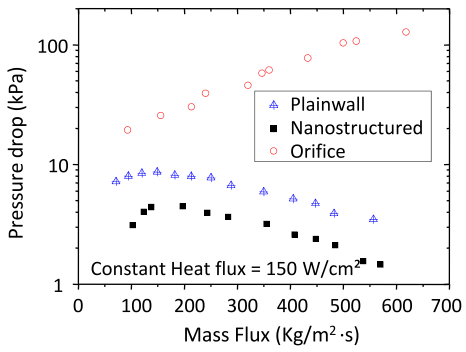

Fig. 1. Comparisons of pressure drop between plain-wall microchannels with & without *IRs* and the *SiNW* microchannels.

The density of the exit two-phase flow, $\rho_{2\phi,o}$, is estimated by

$$\rho_{2\phi,o} = \alpha \cdot \rho_v + (1-\alpha)\cdot \rho_l \quad (3)$$

where α is the void faction, which can be estimated by Eq. (13).

The inlet minor losses was estimated from the model developed in [27]

$$\Delta p_i = \rho_l \frac{\bar{u}_{l,i}^2}{2}\frac{1-\beta\cdot\tau^2\cdot C_C^2 - 2C_C + 2C_C\cdot K_d}{C_C} \quad (4)$$

The exit minor losses was calculated using an equation developed by Abdelall [27]:

$$\Delta p_o = \rho_v \frac{\bar{u}_{v,o}}{2}\left[\frac{1-2K_d\cdot\tau+\tau^2(K_d-1)}{2} - (1-\tau^2)\right] \quad (5)$$

where the parameter, C_C, is given by Geiger [28],

$$C_C = 1 - \frac{1-\tau}{2.08(1-\tau)+0.5371} \quad (6)$$

From Eq. 4, 5, $\bar{u}_{l,i}$ and $\bar{u}_{v,o}$ represent the average liquid velocities at inlet and exit, respectively, and were estimated as $\bar{u}_{l,i} = \dot{m}/(A_l\cdot\rho_l)$ and $\bar{u}_{v,o} = \dot{m}\cdot\chi_e/(A_v\cdot\rho_v)$. The momentum correction factor, $K_d = 1.33$, was used for laminar flow. τ is the flow area contraction ratio.

The pressure drop of the plenum chambers consists of two components:

$$\Delta p_{plenum} = \Delta p_{i,plenum} + \Delta p_{o,plenum} \quad (7)$$

where the pressure drop of the inlet plenum was estimated from

$$\Delta p_{i,plenum} = f_{plenum}\cdot\rho_l\frac{L_{i,plenum}}{D_{i,plenum}}\frac{\bar{u}_{plenum}^2}{2} \quad (8)$$

and the pressure drop of the exit plenum was estimated from

$$\Delta p_{o,plenum} = f_{plenum}\cdot\rho_v\frac{L_{o,plenum}}{D_{o,plenum}}\frac{\bar{u}_{plenum}^2}{2} \quad (9)$$

where L_{plenum} is the length of the plenums; and D_{plenum} is the hydraulic diameter of the plenums. The friction factor was calculated as

$$f_{plenum} = \frac{C_f}{\mathrm{Re}_{plenum}} \tag{10}$$

where C_f was adopted from [29].

The pressure drop of the flow distributors is given by

$$\Delta p_{distributor} = N \cdot f_{cross} \cdot \rho_l \left(\frac{S_T}{S_T - D_{pin}}\right)^2 \frac{\bar{u}^2_{plenum}}{2} \tag{11}$$

where N is the number of pin fins in a single row of flow distributers; f_{cross} was estimated by Gunther and Shaw's method [30]; and S_T is the transverse pitch; and D_{pin} is the hydraulic diameter of pin fins.

In this experimental study, the Reynolds number of vapor flow under a single annular flow is defined as,

$$\mathrm{Re} = \frac{\rho_v (u_v - u_l) D_h}{\mu_v} \tag{12}$$

where μ_v is the dynamic viscosity of vapor.

3. Results and discussion

Hydraulic characteristics in the single annular flow boiling regime were studied. The enhancement mechanisms of *CHF* and the reduced pressure drop are discussed.

3.1. The reduced pressure drops in SiNW microchannels

The overall pressure drop vs. mass flux measured in *SiNW* microchannels and plain-wall microchannels with or without *IRs* are compared in Fig. 1. The major dimensions of microchannels such as height, width, length and number of microchannels in these three configurations are identical. *IRs* usually lead to a significant increase of the pressure drop [31] (Fig. 1). The pressure drops in plainwall microchannels are significantly lower without *IRs*. As illustrated in Fig. 1, the pressure drop in *SiNW* microchannels was significantly reduced by approximately 48% compared to that in smooth-wall microchannels under similar working conditions.

As shown in Fig. 1, the trend of the pressure drop vs. mass flux (Δp–G) curve in microchannels with *IRs* differs from these in smooth-wall and *SiNW* microchannels. For a given heat flux, the pressure drop of microchannels with *IRs* decreases with the mass flux reduction because the major pressure drop is dominated by single-phase flow resistance from IRs. Single-phase flow resistance is governed by the fluid velocity and viscosity. It is straightforward that the fluid velocity decreases with decreasing mass flux; while viscosity decreases because of the resulting higher wall temperature. On the contrary, the pressure drop of microchannels without *IRs* is dominated by two-phase flows, which has a strong relationship with two-phase flow regimes and is known to vary with the vapor qualities [29]. For a given constant heat flux, the mass flux reduction increases the vapor quality and leads to higher pressure drop [20,21]. This result implies that the single two-phase flow pattern enabled by *SiNWs* in microchannels plays a critical role in determining pressure drop. Moreover, the frictional pressure drop, as a major part of the total pressure drop of microchannels, is affected by several hydrodynamic characteristics including liquid entrainment, liquid film renewal and flatness of vapor–liquid interfaces. The experimental and theoretical results on these properties are discussed below.

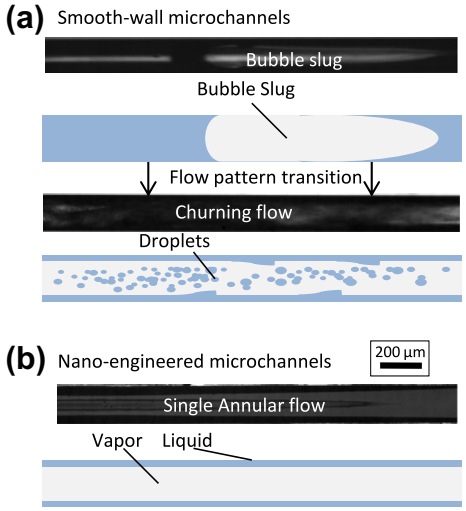

Fig. 2. Major differences in the flow structure between traditional flow boiling regimes and the single annular flow in microchannels. (a) Slug and churning flows in plain-wall microchannels. (b) The single annular flow in *SiNW* microchannels.

3.2. Key differences between the traditional flow patterns and the single annular flow in microchannels

The key differences in the flow structures between microchannels with smooth-walls and *SiNW* walls are shown in Fig. 2. Fabricated from polished silicon wafers by deep reactive-ion etching *(DRIE)*, the roughness ranges from 3 nm to 300 nm in smooth-wall microchannels [32,33]. The contact angle between *DI* water and smooth *Si* surface is between 40° and 60° as a result of the native oxide layers [34]. As shown in Fig. 2a, capillary pressure is generated at vapor–liquid interfaces on vapor slugs in smooth-wall microchannels. The transition of slug flow into churn flows occurs when vapor quality and superficial vapor velocity increases [35,36].

However, with *SiNWs* etched on the inner walls in microchannels, the microchannel walls were modified into super-hydrophilic with an apparent contact angles of less than 0.1° using the Wenzel effect [37]. Moreover, the inner wall peak-to-peak roughness was significantly increased to approximate 5 μm, i.e., microscale wicks, where high capillary pressure can be generated by the superhydrophilic *SiNWs*. As a result, laminar liquid and vapor flows are separated and hence a new single annular flow pattern was formed (Fig. 2b) [38]. A significant difference between the fluid and the vapor superficial velocities was derived. Consequently, the multiple and transitional two-phase flow patterns/regimes [35,36,39–41] (Fig. 2a) were reduced into a single annular flow boiling regime (Fig. 2b) in a periodic manner [38].

In traditional microchannel configurations, annular two-phase flow only occurs at a high superficial vapor/gas velocity [42]. However, in the new single annular flow boiling regime enabled by superhydrophilic *SiNWs* (Fig. 3a), such an annular flow prevails over the entire flow boiling domain, i.e., from the onset of flow boiling (*ONB*) to *CHF* conditions [38]. Note that the new single annular flow is periodic, i.e., the hydraulic diameter of the vapor core expands periodically (Fig. 3a), which is different from the traditional annular flows [36]. Additionally, the mechanism that governs entrainment fraction could be different between the traditional (Fig. 3b) and the new (Fig. 3a) annular flows. There are four basic types of entrainment mechanisms in traditional two-phase flows according to experimental observations [43]. These include roll wave, wave undercut, bubble burst and liquid impingement. In the traditional annular flow, droplet entrainment is primarily determined by the shearing-off crest of roll waves [44].

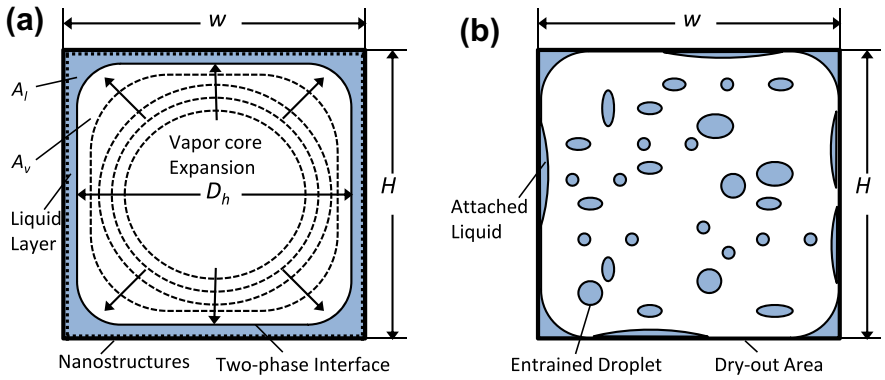

Fig. 3. The schematic of ideal flow structures in the single annular and traditional churning/annular flows in a cross-sectional view. (a) The periodic expansion of the vapor core with a reduced amount of droplets in the single annular flow. (b) Entrained droplets in the churning flow.

However, bubble burst should be the primary entrainment mechanism in the single annular flow since the liquid–vapor interface induced by *SiNWs* is assumed to be flat and smooth because of the high surface tension force induced by superhydrophilic *SiNWs* (Fig. 7).

3.3. The impacts of two-phase flow patterns on pressure drops in microchannels

The primary flow boiling regimes in microchannels with smooth walls and *SiNWs* are compared in Fig. 4b. The frictional pressure drop was plotted as a function of exit vapor quality, χ, and Reynolds number, Re, in Fig. 4b and c, respectively.

As shown in Fig. 4a, the total pressure drop, Δp_{total}, as a function of effective heat flux, q''_{eff}, were directly measured in this experimental study. A significant reduction of total pressure drops as a result of the single annular flow was demonstrated. The frictional pressure drop, $\Delta p_{f,\exp}$, of two-phase flow in *SiNW* microchannels were reduced by deducting other components from the total pressure drops. The major reason behind the significantly reduced pressure drop is because of the reduced frictional pressure drop (Fig. 4c), which is imposed by shear stress at the liquid–vapor interfaces. Particularly, the frictional pressure drop is dominant in the annular flow.

Compared to multiple flow boiling regimes in the smooth-wall microchannels, friction was greatly reduced in the single annular flow regime enabled by *SiNWs* in microchannels with mass fluxes ranging from 160 to 303 kg/m^2 s and exit vapor quality, χ, ranging from nearly 0–0.53 as illustrated in Fig. 4b. This was also observed in previous studies: the formation of a smooth liquid layer created by the capillarity on superhydrophilic surfaces can reduce pressure drop [45,46]. However, the relationship between the flow pattern and the reduced pressure drop is still not well established. In Fig. 4c, the frictional pressure drop is also plotted as a function of Reynolds number. It appears that the friction pressure drops are well correlated by the Reynolds number. The two-phase pressure drop during the entire flow boiling was reduced by approximately 48% compared to smooth-wall microchannels for a given Reynolds number as shown in Fig. 4c.

3.4. Analysis of frictional pressure drop reduction

A theoretical study was conducted to reveal possible mechanisms that determine the significant pressure drop reduction. Experimental results are compared to two ideal two-phase flow models, i.e., ideal annular and mixing flows (homogeneous flows) as shown in Fig. 3a and b. By assuming a pure vapor core (i.e., without droplets), a separated flow model was adopted to present the "ideal" annular flow as shown in Fig. 3a [2]. A homogeneous two-phase flow model (Fig. 3b) was used to represent ideally mixed liquid and vapor flows [2].

While modeling the two-phase pressure drops in the single annular flow, assumptions are made as follows: (1) a quasi-steady state is used to represent the time average pressure drop; (2) the flow resistance from the high velocity vapor contained by the vapor core is dominant; (3) the profile of the vapor core is concentric; (4) reverse flow is effectively suppressed, i.e., one-way vapor flows, as illustrated in Fig. 7 in the Part I; (5) the vapor flow and liquid flow are laminar since Reynolds number is less than 2100; (6) at the inlet, the flow is saturated liquid (i.e., $\chi = 0$); (7) uniform heat flux; and (8) the effects of the glass side wall are ignored (Fig. 3a).

3.4.1. Separated flow model

The local void fraction of two-phase flow can be estimated according to

$$\alpha = 1/\left(1 + \frac{1-\chi}{\chi}\frac{\rho_v}{\rho_l}S\right) \tag{13}$$

where S is the slip ratio. The superficial velocity of the vapor, u_v, in the separated annular flow model is significantly higher than that of the liquid flow. Assuming that liquid droplet is not entrained in the central vapor core of an ideal annular flow, a void fraction model can be developed based on minimum kinetic energy of the annular flow proposed by Zivi [42]. This model assumes the total kinetic energy of vapor and liquid in steady state tends to be a minimum. By minimizing kinetic energy, the slip ratio become $S = (\rho_l/\rho_v)^{1/3}$. Fig. 5 suggests that this model can well predict the liquid profile in the single annular flow. Local void fraction measurements (not obtained in this study) can greatly improve the modeling efforts.

Since the heat flux is uniform, the local vapor mass flow rate, $\dot{m}_v$, increases linearly along the flow direction, z, as a result of a constant, P_{eff},

$$\dot{m}_v = \frac{z}{L}\frac{P_{eff}}{h_{fg}} \tag{14}$$

where L is the length of microchannel and h_{fg} is the latent heat of vaporization. Then local vapor quality was estimated from $\chi = \dot{m}_v/\dot{m}$, where, $\dot{m}$ is the total mass flow rate.

In a quasi-steady state, vapor and liquid superficial velocities in the ideal annular flows can be estimated from

$$u_v = \frac{\dot{m}\cdot\chi}{A_v\cdot\rho_v} \tag{15}$$

and,

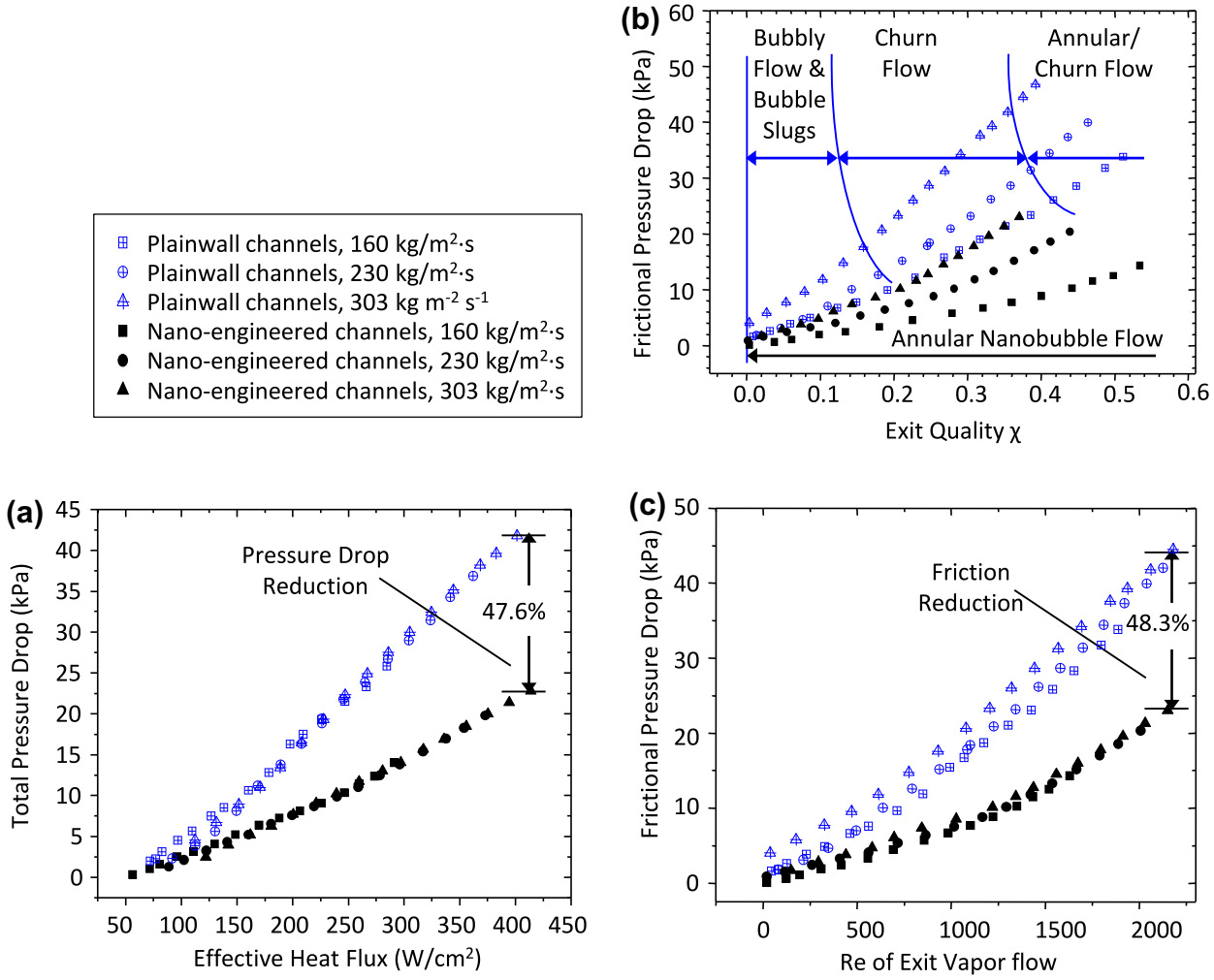

Fig. 4. Comparisons of pressure drop under traditional flow boiling regimes and the single annular regime. (a) Total pressure drop as a function of effective heat fluxes. (b) Frictional pressure drop vs. exit vapor quality is plotted [51]. (b) Frictional pressure drop vs. Reynolds number based on exit vapor flow is plotted.

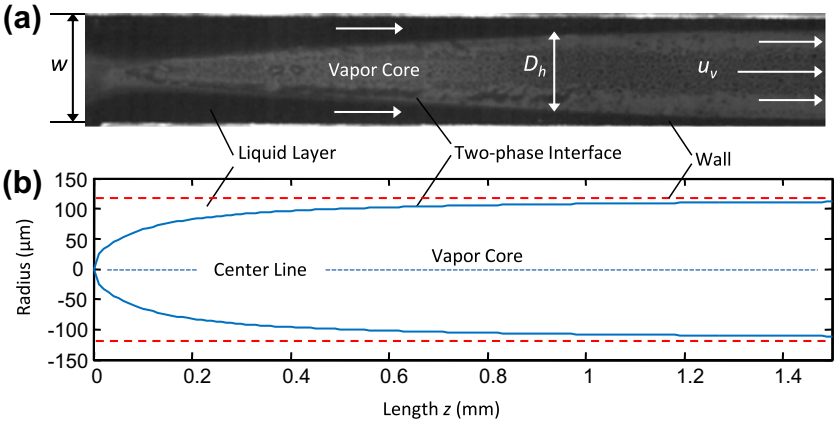

Fig. 5. A typical flow structure in the lateral direction in the single annular flow. (a) The top-viewed image of single annular flow. (b) The modeled profile of flow structure in the single annular flow.

$$u_l = \frac{\dot{m} \cdot (1-\chi)}{A_l \cdot \rho_l} \tag{16}$$

where the cross-section area of the vapor core is $A_v = \alpha \cdot A_c$ and the remaining area of the annular liquid is $A_l = (1-\alpha) \cdot A_c$ (Fig. 2a). A_c is the cross-section area of a single microchannel. The hydraulic diameter of the vapor core was estimated from $D_h = 2\sqrt{A_v/\pi}$ or:

$$D_h \approx 2\sqrt{\frac{A_v}{A_c}}\frac{WH}{(W+H)} \tag{17}$$

where W and H are the width and height of microchannel, respectively.

By assuming a laminar and incompressible flow, a differential equation for the frictional pressure drop for ideal annular flows was derived

$$\Delta p_{f,annular} = 0.5 \int_0^L \frac{f \cdot \rho_v \cdot (u_v - u_l)^2}{D_h} dz \tag{18}$$

where the Fanning friction factor is given by $f = C_f/\mathrm{Re}$. Reynolds number is defined in Eq. (12). C_f was assumed to be 58 for a rectangle vapor core or 64 for a round vapor core in fully developed laminar flow.

3.4.2. Homogenous flow model

Using the average viscosity defined by McAdams [47], the mean viscosity, density, and velocity of the ideal two-phase mixture can be calculated as

$$\begin{aligned} \mu_m &= [z/\mu_v + (1-z)/\mu_l]^{-1} \\ \rho_m &= \alpha\rho_v + (1-\alpha)\rho_l \\ u_m &= \dot{m}/(\rho_m A_c) \end{aligned} \tag{19}$$

In this model, the two-phase mixing flow was assumed as a homogeneous flow so that the slip ratio, S, is 1. The pressure gradient can be expressed as follows:

$$\Delta p_{f,mixture} = 0.5 \int_0^L \frac{f_m \cdot \rho_m \cdot u_m^2}{D_h} dz \tag{20}$$

where $f_m = C_f/\mathrm{Re}_m$ and $\mathrm{Re}_m = \rho_m \cdot u_m \cdot D_h/\mu_m$.

As shown in Fig. 6, from the theoretical modeling, the homogeneous two-phase mixing flow has the maximum pressure drop; while the ideal annular flow model has the lowest pressure drop. The experimental results from the single annular flow boiling regime were between the two models' results. Since the frictional pressure drop is determined by the interactions between fluids and walls as well as between liquid and vapor flows, the pressure drop can be reduced by reducing these contact areas, for example, through separating liquid and vapor flows, i.e., inducing annular flows [2,48]. Thus, the separation of two-phase flows is the primary reason in reducing pressure drop when multiple flow boiling regimes are reduced into a single annular flow. Additionally, the higher pressure drop in the single annular flow than that in the ideal annular flow should come from the higher density of vapor core resulting from bubble burst as discussed in Section 3.2.

3.5. Profile of liquid–vapor interface on SiNW surfaces

The two-phase flow in microchannels is dominated by shear stress and capillary pressure. By comparing the shear stress with the capillary pressures in microchannels with and without nanowires, the dominating factors in two-phase flow are discussed in this study.

The interfacial stress was estimated from frictional pressure drop

$$\sigma_i = \frac{\Delta p_f \cdot D_h}{4L} \tag{21}$$

The capillary pressure was estimated from

$$\Delta p_c = \frac{4\gamma \cdot \cos\theta}{d_n} \tag{22}$$

where γ is surface tension; θ is the contact angle; and d_n is the characteristic length scale. Both the hydraulic diameter of the microchannels and the average diameter of the wall cavities created by the *SiNWs* can be used to define d_n.

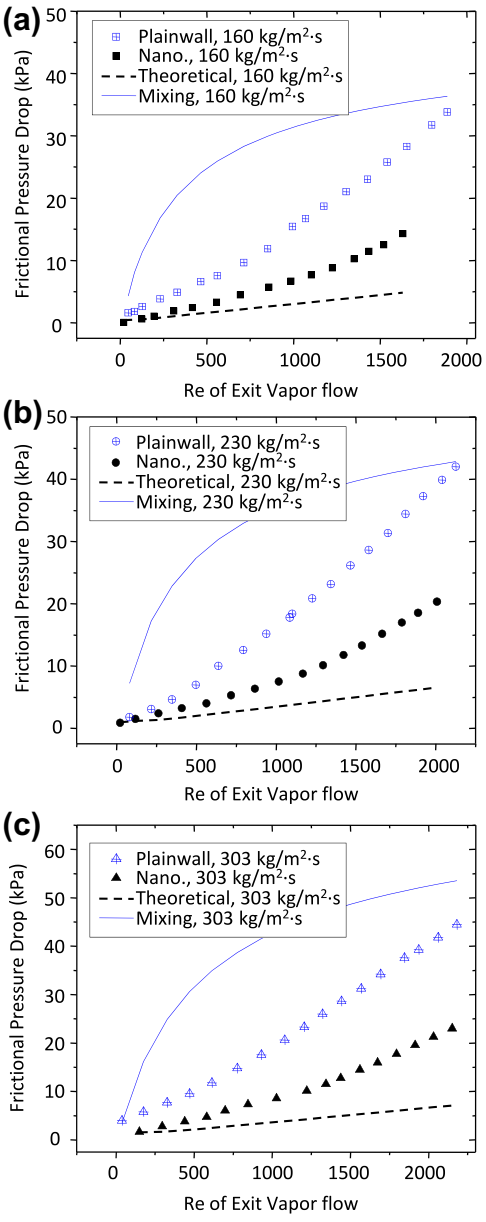

Fig. 6. Analysis of pressure drop reduction in a single annular flow. (a) G = 160 kg/m^2 s, (b) G = 230 kg/m^2 s, and (c) G = 303 kg/m^2 s.

As illustrated in Fig. 7a, the capillary pressure generated by superhydrophilic *SiNWs* (Eq. (22)) is approximately five orders of magnitude higher than the shear stress imposed by vapor flows, the liquid is firmly attached to the *SiNWs* and the profile become smooth and nearly flat (Fig. 7b). As a result, the droplet entrainment by the shearing-off crest of roll waves is dramatically reduced. In smooth microchannels, droplet entrainment is primarily determined by the shearing-off crest of roll waves [44] as shown in Fig. 7c. Bubble burst is probably the primary entrainment mechanism in the single annular flow.

The shear stress (estimated from frictional pressure drops) in *SiNW* microchannels is two to five orders of magnitude smaller than the capillary pressures generated on superhydrophilic *SiNWs* (Fig. 7a). On the other hand, Fig. 7 suggests that shear stress at the liquid–vapor interfaces (contact angle, ~60°) and the capillary pressure generated in the cross-sectional direction have the same order of magnitude. As a result, wavy liquid–vapor interfaces are

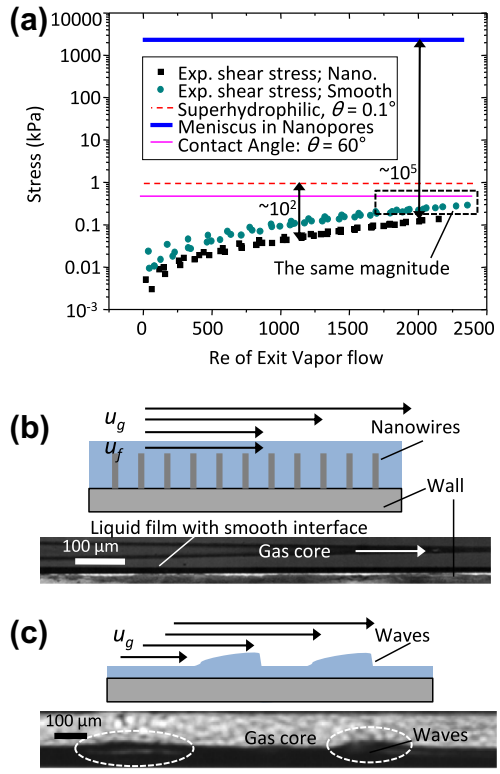

Fig. 7. Effects of interfacial shear stress and capillary pressure on the profile of liquid–vapor interface during flow boiling in microchannels. (a) Average shear stresses reduced from experiments are plotted as a function of Reynolds number of exit vapor flow and compared to capillary pressure generated in the cross-sectional direction in smooth-wall microchannels and in the wall-plane on *SiNW* walls. (b) Image and schematic of nearly flat liquid–vapor interface in the single annular flow in the *SiNW* microchannels. (c) Image and schematic of wavy liquid–vapor interface in smooth-wall microchannels.

formed, and hence, shearing-off crest of roll waves dominates droplet entrainment (Fig. 7c).

Visualization study was also conducted to experimentally validate the liquid–vapor interface profiles in two microchannel configurations. The smooth and nearly flat profiles of the liquid–vapor interfaces were visualized in the microchannels with *SiNWs* (Fig. 7b); while the wavy profiles of the liquid–vapor interfaces were typical in microchannels with smooth walls (Fig. 7c).

3.6. Enhanced CHF conditions in the single annular flow

As illustrated in Fig. 8, *CHF* in smooth-wall microchannels reached at approximately 155 W/cm^2 because of pre-mature *CHF* conditions [49]. On the other hand, in the *SiNW* microchannels, *CHF* of 491 W/cm^2 was achieved at a moderate mass flux of G = 389 kg/m^2 s without using *IRs*. As shown in Fig. 8, when compared to plain-wall microchannels without using *IRs*, *CHF* in the single annular flow enabled by *SiNWs* is 317% higher. Additionally, when compared to microchannels with *IRs*, *CHF* in the new flow boiling regime [38] was almost the same when the mass fluxes were less than 200 kg/m^2 s. A reduction of 6.4–25.8% was observed for mass fluxes ranging from 200 to 400 kg/m^2 s, but with a reduced pressure drop (Fig. 1).

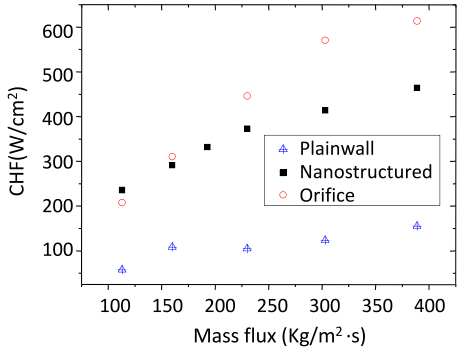

Fig. 8. Comparison of *CHF* between plain-wall microchannels with & without *IRs* and *SiNW* microchannels.

Without using *IRs*, the significantly enhanced *CHF* in microchannels with hydrophilic *SiNWs* is a result of the single flow boiling pattern, which radically eliminated one of the primary *CHF* mechanisms, i.e., the stochastic nature of flow pattern transitions. Under the single annular flow, the liquid supply at local and global levels has been substantially improved. As shown in Fig. 9a, local liquid supply was greatly improved by the capillary flows induced by the superhydrophilic *SiNWs*, and hence delayed local dry-out that occurs at low heat fluxes in the smooth-wall microchannels [3]. More importantly, global liquid supply, as shown in Fig. 9b, was significantly improved because of the high frequency (at approximately 36 Hz) liquid renewal over the entire channel resulted from the collapse of the vapor core [38].

Mechanisms triggering *CHF* in two-phase flow are roughly classified into two categories: departure from nucleate boiling (*DNB*) at a low vapor quality and annular film dry-out (*AFD*) at a high vapor quality [50]. According to the visualization study and the high vapor quality, the *CHF* mechanism of the single annular flow is *AFD*. As illustrated in Fig. 10, flow boiling approached *CHF* conditions once the global rewetting motions stopped. Prior to *CHF* (Fig. 10), the vapor core did not collapse completely as observed in Fig. 9b. Fig. 10a showed that the entire channel was quickly devoid of coolant and filled with vapor at a heat flux of 150 W/cm^2 for a low mass flux of 90 kg/m^2 s. Under *CHF* conditions, rewetting flows can only reach the areas near the entrance and cannot approach the

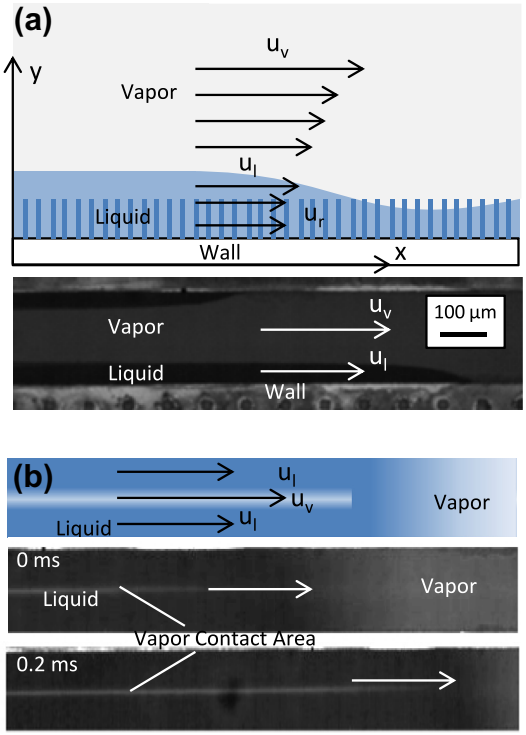

Fig. 9. Improved global and local liquid supply in the *SiNW* microchannels. (a) Improved local rewetting by capillarity along *SiNW* walls. (b) Improved global liquid supply by rapid rewetting. Thin liquid film was still observed prior to *CHF* conditions.

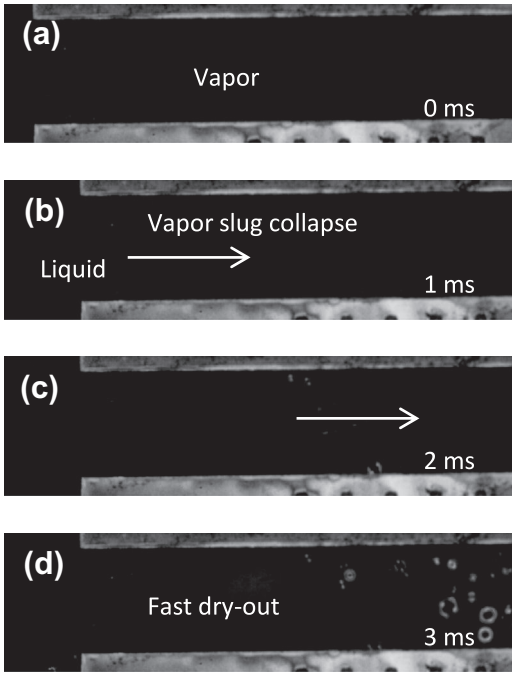

Fig. 10. Flow structure near *CHF* conditions in the *SiNW* microchannels. Images were captured by a high-speed camera at 1000 frames per second. Working condition: q''_{eff} = 150 W/cm^2, $\dot{m}$ = 90 kg/m^2 s. (a) Liquid films were not visualized and microchannel was filled by vapor. (b) The vapor slug partially collapsed. (c) Microchannel cannot be fully rewetted. (d) Continuous liquid films were broken. Expanding dry areas on walls led to an escalation of wall temperatures.

downstream as shown in Fig. 10b and c. The continuous liquid film induced by capillarity was also interrupted. The failure to establish a stable liquid supply caused dry-out of the entire microchannels.

According to current visualization studies, CHF conditions are randomly triggered in a microchannel array. However, the rapid local dryout in one channel usually leads to the dryout of its neighboring channels in a short time. Firstly, the fast-growing confined vapor slug in a channel would rapidly effect its neighboring channels through bubble interactions between channels. This type of interactions is known to be an important reason resulting in flow instabilities and premature CHF conditions [3]. The other reason is the quick temperature response of the 200 μm thick wall. The jump of temperature in a channel can quickly elevate the temperature in its neighboring channels.

4. Conclusion

Hydraulic characteristics of the single annular flow were systematically studied. Frictional pressure drop was significantly reduced in the new flow boiling pattern compared to smooth-wall microchannels under similar working conditions. The separated vapor and liquid flows and flattened liquid–vapor interfaces under the single annular flow are the primary reason for ~48% reduction in the pressure drop. Specifically, the reduced entrainment droplets overcoming the shearing-off crest of the roll waves was observed because of the high capillary pressure generated by superhydrophilic *SiNWs*. The enhanced *CHF* in the new flow pattern was a result of the elimination of the flow pattern transition and the greatly improved global and local liquid supply.

Acknowledgements

This work was supported by the startup funding of the University of South Carolina (USC) and the U.S. Department of Defense, Office of Naval Research (ONR) under the Grant N000140810080 (Program Officer Mrs. Sharon Beermann-Curtin) and the Grant N000141210724 (Program Officer Dr. Mark Spector). The authors would like to thank Dr. C.J. Kuo for his help in microfabrication and building testing system. SEM figures in this study were taken in the Electron Microscopy Center at University of South Carolina. Part of the microfabrication was performed at the Cornell Nanoscale Facility (CNF), a member of the National Nanotechnology Infrastructure Network of United States, which is supported by the National Science Foundation under the Grant ECS-0335765.

References

[1] P. Cheng, H.Y. Wu, F.J. Hong, Phase-change heat transfer in microsystems, J. Heat Transfer-Trans. ASME 129 (2) (2007) 101–108.
[2] R.T. Lahey, F.J. Moody, The Thermal-hydraulics of a Boiling Water Nuclear Reactor, second ed., American Nuclear Society, La Grange Park, Illinois, USA, 1977.
[3] A.E. Bergles, S.G. Kandlikar, On the nature of critical heat flux in microchannels, J. Heat Transfer-Trans. ASME 127 (1) (2005) 101–107.
[4] A. Kosar, C.J. Kuo, Y. Peles, Suppression of boiling flow oscillations in parallel microchannels by inlet restrictors, J. Heat Transfer-Trans. ASME 128 (3) (2006) 251–260.
[5] H.J. Lee, D.Y. Liu, S.-c. Yao, Flow instability of evaporative micro-channels, Int. J. Heat Mass Transfer 53 (9–10) (2010) 1740–1749.
[6] B. Schneider, A. Kosar, C.J. Kuo, C. Mishra, G.S. Cole, R.P. Scaringe, Y. Peles, Cavitation enhanced heat transfer in microchannels, J. Heat Transfer-Trans. ASME 128 (12) (2006) 1293–1301.
[7] L. Guohua et al., Seed bubbles trigger boiling heat transfer in silicon microchannels, Microfluid. Nanofluid. (2009).
[8] L. Guohua, X. Jinliang, Y. Yongping, Z. Wei, Active control of flow and heat transfer in silicon microchannels, J. Micromech. Microeng. 20 (4) (2010) 045006.
[9] J. Xu, G. Liu, W. Zhang, Q. Li, B. Wang, Seed bubbles stabilize flow and heat transfer in parallel microchannels, Int. J. Multiphase Flow 35 (8) (2009) 773–790.
[10] F. Yang, X. Dai, C.-J. Kuo, Y. Peles, J. Khan, C. Li, Enhanced flow boiling in microchannels by self-sustained high frequency two-phase oscillations, Int. J. Heat Mass Transfer 58 (1–2) (2013) 402–412.
[11] F. Yang, X. Dai, C. Li, High frequency microbubble-switched oscillations modulated by microfluidic transistors, Appl. Phys. Lett. 101 (7) (2012). 073509–073504.
[12] L. Chun Ting, P. Chin, A highly stable microchannel heat sink for convective boiling, J. Micromech. Microeng. 19 (5) (2009) 055013.
[13] B.R. Fu, M.S. Tsou, C. Pan, Boiling heat transfer and critical heat flux of ethanol–water mixtures flowing through a diverging microchannel with artificial cavities, Int. J. Heat Mass Transfer 55 (5–6) (2012) 1807–1814.
[14] P.H. Lin, B.R. Fu, C. Pan, Critical heat flux on flow boiling of methanol–water mixtures in a diverging microchannel with artificial cavities, Int. J. Heat Mass Transfer 54 (15–16) (2011) 3156–3166.
[15] L. Po Chang, P. Chin, Boiling heat transfer and two-phase flow of water in a single shallow microchannel with a uniform or diverging cross section, J. Micromech. Microeng. 18 (2) (2008) 025005.
[16] G. Wang, P. Cheng, A.E. Bergles, Effects of inlet/outlet configurations on flow boiling instability in parallel microchannels, Int. J. Heat Mass Transfer 51 (9–10) (2008) 2267–2281.
[17] A. Mukherjee, S.G. Kandlikar, The effect of inlet constriction on bubble growth during flow boiling in microchannels, Int. J. Heat Mass Transfer 52 (21–22) (2009) 5204–5212.
[18] S.G. Kandlikar, W.K. Kuan, D.A. Willistein, J. Borrelli, Stabilization of flow boiling in microchannels using pressure drop elements and fabricated nucleation sites, J. Heat Transfer 128 (4) (2006) 389–396.
[19] A. Cavallini, D. Del Col, M. Matkovic, L. Rossetto, Frictional pressure drop during vapour–liquid flow in minichannels: modelling and experimental evaluation, Int. J. Heat Fluid Flow 30 (1) (2009) 131–139.
[20] X. Dai, F. Yang, R. Fang, T. Yemame, J.A. Khan, C. Li, Enhanced single and two-phase transport phenomena using flow separation in a microgap with copper woven mesh coatings, Appl. Therm. Eng. (0) (2013).
[21] W. Hailei, R.B. Peterson, Enhanced boiling heat transfer in parallel microchannels with diffusion brazed wire mesh, IEEE Trans. Compon. Packag. Technol. 33 (4) (2010) 784–793.
[22] P. Rapolu, S. Son, Characterization of wettability effects on pressure drop of two-phase flow in microchannel, Exp. Fluids 51 (4) (2011) 1101–1108.
[23] H. Trieu Phan, N. Caney, P. Marty, S. Colasson, J. Gavillet, Flow boiling of water in a minichannel: the effects of surface wettability on two-phase pressure drop, Appl. Therm. Eng. 31 (11–12) (2011) 1894–1905.
[24] H.S. Ahn, S.H. Kang, C. Lee, J. Kim, M.H. Kim, The effect of liquid spreading due to micro-structures of flow boiling critical heat flux, Int. J. Multiphase Flow 43 (2012) 1–12.
[25] S. Vafaei, D. Wen, Critical heat flux (CHF) of subcooled flow boiling of alumina nanofluids in a horizontal microchannel, J. Heat Transfer 132 (10) (2010) 102404–102407.

[26] C.J. Kuo, Y. Peles, Flow boiling instabilities in microchannels and means for mitigation by reentrant cavities, J. Heat Transfer-Trans. ASME 130 (7) (2008).
[27] F.F. Abdelall, G. Hahn, S.M. Ghiaasiaan, S.I. Abdel-Khalik, S.S. Jeter, M. Yoda, D.L. Sadowski, Pressure drop caused by abrupt flow area changes in small channels, Exp. Therm. Fluid Sci. 29 (4) (2005) 425–434.
[28] G.E. Geiger, Sudden Contraction Losses in Single and Two-phase Flow, University of Pittsburgh, Pittsburgh, USA, 1964.
[29] R.K. Shah, A.L. London, Laminar Flow Forced Convection in Ducts, Academic Press, New York, 1978.
[30] A.Y. Gunther, W.A. Shaw, A general correlation of friction factors for various types of surfaces in cross flow, Trans. ASME 67 (1945) 643–660.
[31] W.K. Kuan, S.G. Kandlikar, Experimental Study on the Effect of Stabilization on Flow Boiling Heat Transfer in Microchannels, Heat Transf. Eng. 28 (8–9) (2007) 746–752.
[32] S. Chandrasekaran, S. Sundararajan, Effect of microfabrication processes on surface roughness parameters of silicon surfaces, Surf. Coat. Technol. 188–189 (2004) 581–587.
[33] C.J. Kuo, A. Kosar, Y. Peles, S. Virost, C. Mishra, M.K. Jensen, Bubble dynamics during boiling in enhanced surface microchannels, J. Microelectromech. Syst. 15 (6) (2006) 1514–1527.
[34] R. Chen, M.C. Lu, V. Srinivasan, Z. Wang, H.H. Cho, A. Majumdar, Nanowires for enhanced boiling heat transfer, Nano Lett. 9 (2) (2009) 548–553.
[35] S.G. Kandlikar, Fundamental issues related to flow boiling in minichannels and microchannels, Exp. Therm. Fluid Sci. 26 (2–4) (2002) 389–407.
[36] A. Serizawa, Z. Feng, Z. Kawara, Two-phase flow in microchannels, Exp. Therm. Fluid Sci. 26 (6–7) (2002) 703–714.
[37] A. Egatz-Gomez, R. Majithia, C. Levert, K.E. Meissner, Super-wetting, wafer-sized silicon nanowire surfaces with hierarchical roughness and low defects, RSC Adv. 2 (30) (2012) 11472–11480.
[38] F. Yang, X. Dai, Y. Peles, P. Cheng, C. Li, Can multiple flow boiling regimes be reduced into a single one in microchannels?, Appl Phys. Lett. 103 (4) (2013) 043122–043125.
[39] E. Bonaccurso, H.J. Butt, V.S.J. Craig, Surface roughness and hydrodynamic boundary slip of a Newtonian fluid in a completely wetting system, Phys. Rev. Lett. 90 (14) (2003).
[40] L.B. Fore, S.G. Beus, R.C. Bauer, Interfacial friction in gas–liquid annular flow: analogies to full and transition roughness, Int. J. Multiphase Flow 26 (11) (2000) 1755–1769.
[41] M. Sbragaglia, R. Benzi, L. Biferale, S. Succi, F. Toschi, Surface roughness-hydrophobicity coupling in microchannel and nanochannel flows, Phys. Rev. Lett. 97 (20) (2006).
[42] P.F. Vassallo, R. Kumar, Liquid and gas velocity measurements using LDV in air–water duct flow, Exp. Therm. Fluid Sci. 19 (2) (1999) 85–92.
[43] M. Ishii, M.A. Grolmes, Inception criteria for droplet entrainment in two-phase concurrent film flow, AIChE J. 21 (2) (1975) 308–318.
[44] T. Okawa, T. Kitahara, K. Yoshida, T. Matsumoto, I. Kataoka, New entrainment rate correlation in annular two-phase flow applicable to wide range of flow condition, Int. J. Heat Mass Transfer 45 (1) (2002) 87–98.
[45] J. Rovinsky, N. Brauner, D. Moalem Maron, Analytical solution for laminar two-phase flow in a fully eccentric core-annular configuration, Int. J. Multiphase Flow 23 (3) (1997) 523–543.
[46] D. Li, G.S. Wu, W. Wang, Y.D. Wang, D. Liu, D.C. Zhang, Y.F. Chen, G.P. Peterson, R. Yang, Enhancing flow boiling heat transfer in microchannels for thermal management with monolithically-integrated silicon nanowires, Nano Lett. (2012).
[47] W.H. McAdams, W.K. Woods, L.C. Heroman, Vaporization inside horizontal tubes-III. Benzene–oil mixtures, Trans. ASME 64 (1942) 193.
[48] H. Chen, J. Xu, Z. Li, F. Xing, J. Xie, W. Wang, W. Zhang, Flow pattern modulation in a horizontal tube by the passive phase separation concept, Int. J. Multiphase Flow 45 (2012) 12–23.
[49] T. Zhang, T. Tong, J.-Y. Chang, Y. Peles, R. Prasher, M.K. Jensen, J.T. Wen, P. Phelan, Ledinegg instability in microchannels, Int. J. Heat Mass Transfer 52 (25–26) (2009) 5661–5674.
[50] J.G. Collier, J.R. Thome, Convective Boiling and Condensation, third ed., Oxford Engineering Science, 1996.
[51] G. Hetsroni, A. Mosyak, Z. Segal, E. Pogrebnyak, Two-phase flow patterns in parallel micro-channels, Int. J. Multiphase Flow 29 (3) (2003) 341–360.